

THE FLEXURAL FATIGUE BEHAVIOR OF HONEYCOMB SANDWICH COMPOSITES FOLLOWING LOW-VELOCITY IMPACTS

Murat Yavuz Solmaz¹ and tolga topkaya²

¹Affiliation not available

²Batman Universitesi

May 18, 2020

Abstract

This study experimentally investigated the flexural fatigue behaviors of honeycomb sandwich composites subjected to low velocity impact damage by considering the type and thickness of the face sheet material, the cell size and the core height parameters. First, the static strength of undamaged specimens was determined by three-point bending loads, and calculating their fatigue lives; secondly, the fatigue lives of the specimens damaged by low velocity impact tests were then determined. Increasing the face sheet thickness and core height increased the flexural strength, while increasing the cell size decreased the flexural strength. Low velocity impact damage decreased the flexural strength and fatigue lives but increased the damping ratio for all specimens.

Abstract

This study experimentally investigated the flexural fatigue behaviors of honeycomb sandwich composites subjected to low velocity impact damage by considering the type and thickness of the face sheet material, the cell size and the core height parameters. First, the static strength of undamaged specimens was determined by three-point bending loads, and calculating their fatigue lives; secondly, the fatigue lives of the specimens damaged by low velocity impact tests were then determined. Increasing the face sheet thickness and core height increased the flexural strength, while increasing the cell size decreased the flexural strength. Low velocity impact damage decreased the flexural strength and fatigue lives but increased the damping ratio for all specimens.

Keywords : Honeycomb Sandwich Composites; Bending Test; Low Velocity Impact; Fatigue

Introduction

Composites are one of the fundamental materials in today's engineering applications. The reason for that popularity is because they combine high strength with low weight. In particular, sandwich composites are preferred in applications requiring low weight¹⁻³. Usually, aluminum and Nomex honeycomb are used as a core material to produce sandwich composites; on the other hand, carbon fiber-reinforced composites (CFRP) and auxetic materials in various geometries have also been used in recent years³⁻⁶.

Honeycomb sandwich composites are formed by putting thick core structures in between thin and thick plates. The bonding between plates and honeycomb cells is achieved by structural adhesives that have numerous application areas⁷. Honeycomb structures are defined by low weight and high flexural rigidity characteristics, but they are also conveniently used to counter tensile and flexural loads⁸⁻¹⁰.

Unlike metals, composites do not have a homogeneous and isotropic structure. Damage is not seen due to local crack propagation. Fiber damage occurs through the formation of different damage mechanisms like matrix damage and delamination^{11–14}. The most common types of damage observed during honeycomb sandwich composite production are “malformation and adhesive failures”¹⁵. Jen et al. numerically and experimentally investigated the amount of adhesive used between an aluminum honeycomb core and a face sheet on the flexural fatigue behavior of composites. They used three different amounts of adhesive (0.4, 0.7 and 1 kg/m²) and determined that increasing amounts of adhesive increased the flexural strength, and that debonding between the honeycomb core and the face sheet caused permanent fatigue damage¹⁶. Subhani investigated the effect of the curing temperature of the film adhesive – used for bonding honeycomb cores and face sheet material together – on the flexural strength of the composite. The result of the study revealed that the optimum temperature and curing time for the film adhesive was 110°C and 2 hours, respectively¹⁷. In another study performed by Jen et al., their numerical and experimental investigation of four-point bending fatigue behaviors of honeycomb sandwich composites with different face sheet thicknesses, showed that the reason for the resulting damage formed in the specimens was delamination between the core and the face sheet materials¹⁸. Abbadi et al. investigated the fatigue behaviors of undamaged and damaged specimens by using four-point bending loads. The results obtained indicated that the damage formed had no effect on the static strength of specimens¹⁹. Schubel et al. stated that difficult-to-detect damage like delamination formed in sandwich composites after impact caused significant reductions in the strength of specimens²⁰. Belingardi et al. investigated the effect of adhesive failure between cores and face sheet material on the fatigue life of honeycomb sandwich composites and reported that core crushing was observed in the regions of adhesive failure²¹. Shi et al. investigated the effect of aramid fiber-reinforcement of the interface to increase bonding between the honeycomb cores and face sheet material and revealed that aramid fiber-reinforcement increased the strength of the specimen under bending and compression loading²².

In the aviation industry, where honeycomb sandwich composites are primarily used, airplanes are subject to impact damage due to external factors like birds, stone and surface modes. Akatay et al. experimentally investigated the behavior of repetitive low velocity impact on 10 mm-thick sandwich composites produced using an Al 5052 alloy honeycomb core. Results revealed that a 110 Joules of impact energy crushed the specimen at the first impact. More collisions were necessary to crush the specimen as impact energy decreased. A maximum of 81 impacts was found to produce the same damage at an impact energy of 3 Joules²³. Galehdari et al. experimentally, analytically and numerically analyzed static and low velocity impact behaviors of reinforced honeycomb sandwich composites and showed that damage was usually observed in the shape of a “V”; their analysis results were in accordance with experimental results²⁴. Baba experimentally investigated low velocity impact behaviors of curved sandwich composites with a foam core and revealed that curved sandwich composites were stronger than flat sandwich composites under low velocity impact loading²⁵. He et al. investigated the effect of design parameters on the impact behaviors of honeycomb sandwich composites. The parameters affecting impact loading the most were found to be face sheet thickness and honeycomb cell wall thickness, while core height was determined to be the most ineffective parameter²⁶.

To calculate changes in the damping ratio of materials under fatigue loading, hysteresis curves drawn using data obtained from tests can be used²⁷. Another method used in determining the change in damping ratio of a specimen is “damping change”²⁸. Damping is defined as the amount of energy that materials absorb under cyclic stresses²⁹.

In the present study, the damage behaviors of honeycomb sandwich composites were experimentally investigated with three-point bending, low velocity impact, and fatigue before and after impact. The static strengths of specimens were determined by three-point bending loads, and then they were subjected to fatigue tests to determine the fatigue lives of undamaged specimens. Impact damage – a type of damage commonly observed in applications where honeycomb sandwich composites are used – was investigated by low velocity impact testing, and damaged specimens were subjected to fatigue test, and then the effect of impact damage on fatigue lives were investigated.

Material and Methods

The core material of the honeycomb used was Al-3003 alloy. Honeycomb cores were placed in between two different face sheet materials, one Al-5754 and the other a carbon fiber-reinforced composite plate. Adhesion between the face sheet materials and the honeycomb cores was provided by 3M 2216 epoxy-based adhesive.

The honeycomb cores had cell sizes of 6.35 mm and 9.525 mm in diameter (D) and 10 mm, 15 mm and 20 mm in height (T). Face sheet materials had various thicknesses: 0.5 mm, 1 mm and 1.5 mm. These materials produced a composite sample of 80 mm in width and 135 mm in length. The honeycomb sandwich composite layers are shown in Figure 1, while a specimen labeling list and specimen properties for each label are shown in Table 1.

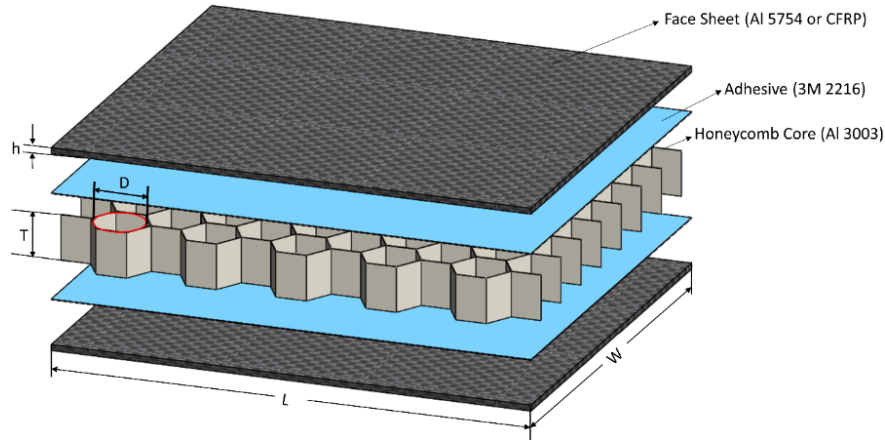


Figure 1. Honeycomb sandwich specimen layers

Table 1 Specimen properties

Specimen codes	Cell size (D) mm	Face sheet material	Core height (T) mm	Face sheet thickness mm (h)
6AL10a	6.35	Aluminum	10	0.5
6AL10b	6.35	Aluminum	10	1
6AL10c	6.35	Aluminum	10	1.5
6AL15b	6.35	Aluminum	15	1
6AL20b	6.35	Aluminum	20	1
9AL10b	9.525	Aluminum	10	1
6CFRP10a	6.35	CFRP	10	0.5
6CFRP10b	6.35	CFRP	10	1
6CFRP10c	6.35	CFRP	10	1.5

Face sheet materials were first ground with 180 grade sandpaper in accordance with the 3M 2216 adhesive user instructions, and then the aluminum plates were cleaned with acetone, while the composite plates were cleaned with isopropyl alcohol.

Jen et al. indicated that an 0.7 kg/m^2 amount of adhesive achieved maximum flexural strength¹⁶; therefore, 7.5 g of adhesive, corresponding to that amount, was applied to the cleaned side of the face sheet materials with a spatula. After applying adhesive to a single face, the samples were kept under a 2.5 kg weight for 24 hours, and then adhesive was applied to the other face. Before performing tests, all specimens were left at room temperature for 1 week to ensure completion of the adhesive curing process.

The mechanical properties of the 3M 2216 adhesive, and the Al-5754 and Al-3003 alloys are shown in Table 2, while the mechanical properties of the CFRP composite are shown in Table 3. E_1 and E_2 are the longitudinal and transverse elastic modulus, ν_{12} is Poisson's ratio, G_{12} is the shear modulus, and X^T and X^C are longitudinal tensile and compressive strengths, respectively. X^C , Y^C and S are longitudinal compressive strength, transverse compressive strength and shear strength, respectively.

Table 2. Mechanical properties of the adhesive, and the Al-5754 and Al-3003 alloys

	Young's Modulus	Poisson's Ratio	Tensile Strength (MPa)
3M 2216 Adhesive	565 MPa	0.47	19.88
Al-5754 Face Sheet	70.3 GPa	0.33	245
Al-3003 Core	68.9 GPa	0.33	131

Table 3. Mechanical properties of the CFRP composite

	E_1 (GPa)	E_2 (GPa)	ν_{12}	G_{12} (GPa)	X^T, Y^T (MPa)	X^C, Y^C (MPa)	S (MPa)
CFRP Face Sheet	83.4	83.5	0.05	6.8	1008	953	125

Static Tests

Bending tests were performed in accordance with the ASTM C393 standard at a 1 mm/min loading rate using Shimadzu Universal test equipment with a 250 kN load cell. During three-point bending tests, load was applied with a 30 mm-diameter cylinder. The span length between the 30 mm-diameter supports was 80 mm. Figure 2 shows the application of load to the specimen.

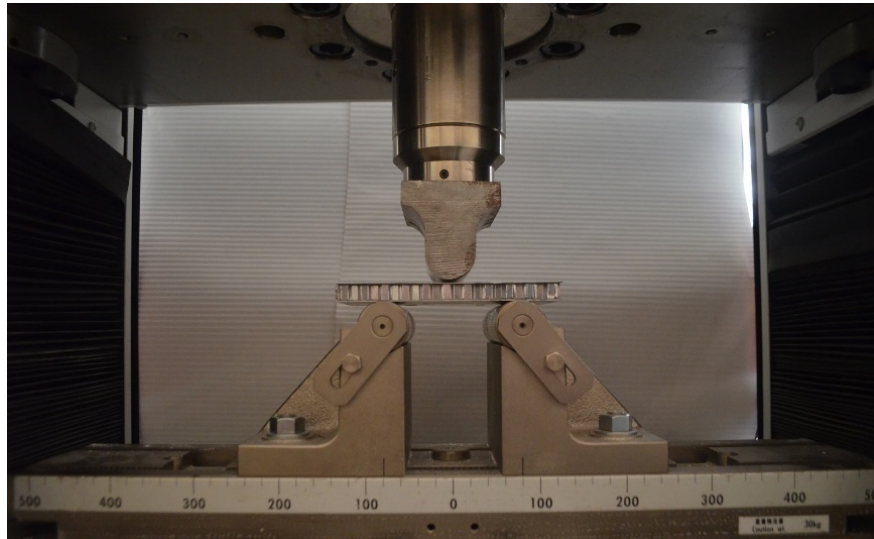


Figure 2. Application of load to specimens during the static test

Impact Tests

Impact tests were carried out using CEAST Fractovis Plus impact test equipment with a capacity of 1800 Joules and a 22 kN load cell. A 12.7 mm diameter steel hemispherical strike face, weighing 5120 grams, was used during these tests. Tests were done at 5 Joule and 10 Joule impact energies. During the impact,

upper and lower supports of 76 mm in diameter were used to hold the specimen. The impact test procedure and the results obtained can be seen in reference ³⁰. Figure 3 shows the post-damage images of specimens 6AL10a, 6AL10b and 6AL10c specimens that were subjected to a low velocity impact test with 5 Joules of impact energy.

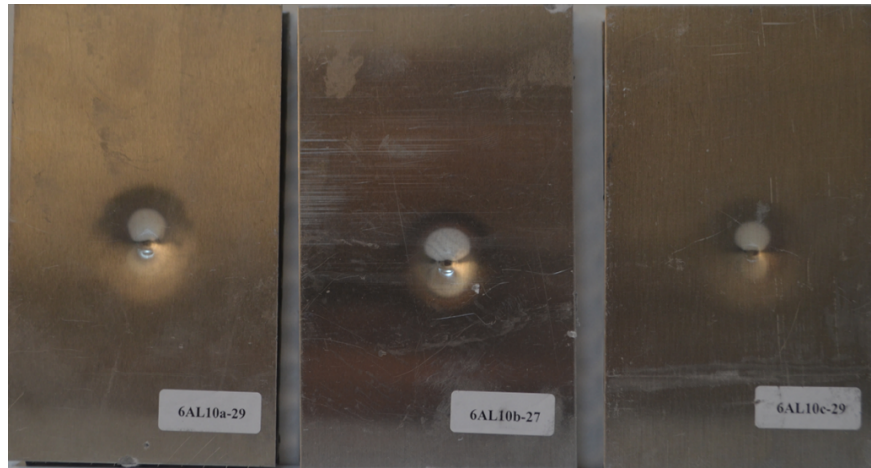
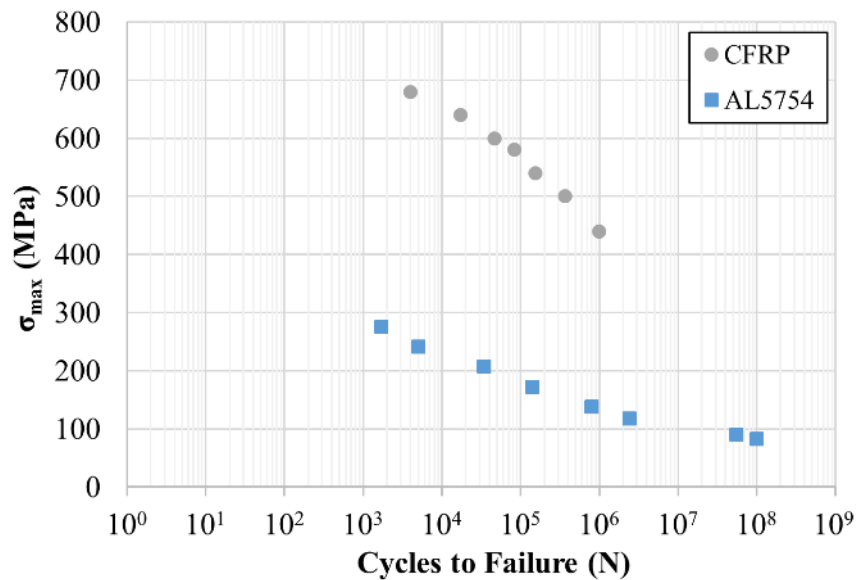


Figure 3. 6AL10a-b-c specimen images obtained after 5 Joules of impact energy

Fatigue Tests

Fatigue tests were conducted using Shimadzu Servo-Hydraulic Fatigue test equipment with a 100 kN load cell. First, the fatigue behaviors of the materials used in producing the sandwich composites were determined using a 5 Hz frequency. Load was applied to specimens as a sine wave and R ($\sigma_{\min}/\sigma_{\max}$) of 0.1 was used. Fatigue tests were performed for aluminum, the 3M 2216 adhesive and the composite materials, for values below static damage loads. Figure 4 shows stress vs. cycles to failure graphs for the Al 5754 face sheet, the 3M 2216 adhesive and the CFRP.



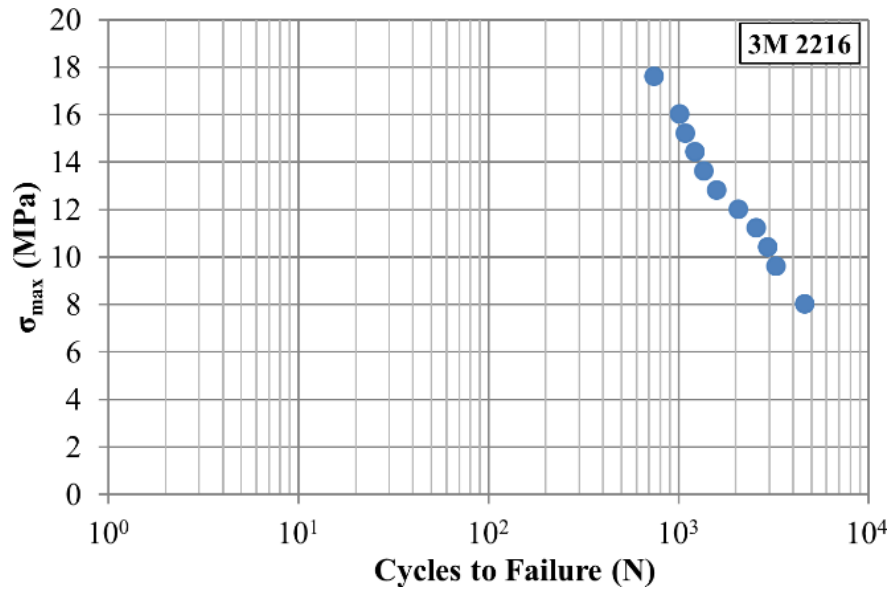


Figure 4. Stress vs. Cycles to failure graphs for the materials used

Results

This study experimentally investigated the effect of preliminary impact damage on the fatigue behaviors of honeycomb sandwich composites. Preliminary impact damage was formed at impact energies of 5 Joules and 10 Joules as a result of low velocity impact tests. The effects of the preliminary impact damage on the strength and fatigue lives of specimens were investigated by bending tests. The results obtained are given below.

4.1. Flexural Tests

Figure 5 shows the images of specimens – with aluminum and CFRP face sheet materials – obtained after three-point bending tests for different face sheet thicknesses. Examining the images, in the model with an aluminum face sheet of 0.5 mm thickness, face wrinkling damage was observed at the first contact point of the cylinder used to apply the load. This damage was seen to be less in the model with a 1 mm face sheet thickness, while it was not seen in the specimen with a 1.5 mm face sheet thickness.

For specimens with a 0.5 mm thick CFRP face sheet, local crushing was dominant in the honeycomb core to which the load was applied. The amount of deflection increased with increasing face sheet thickness and the highest flexural damage was observed in the model with a face sheet thickness of 1.5 mm (Figure 5).

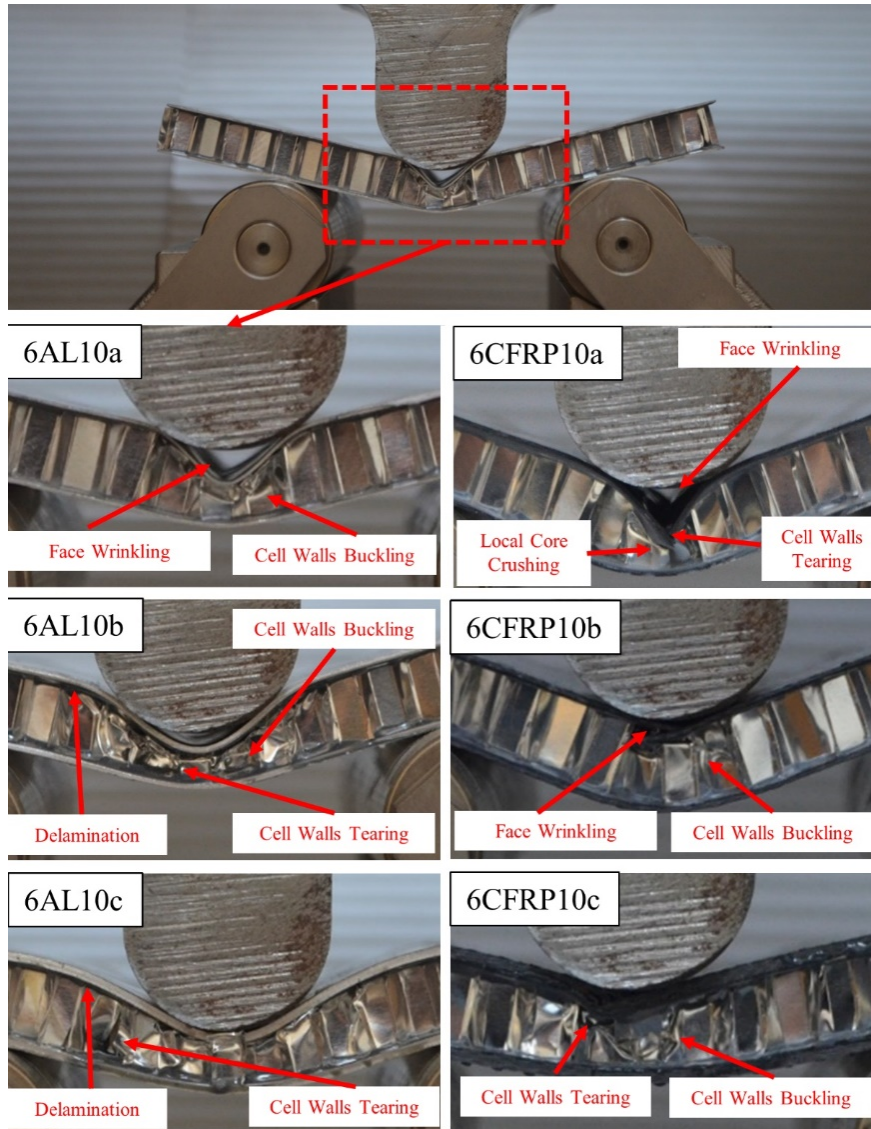


Figure 5. Specimen images obtained after three-point bending tests

There was no surface damage observed in specimen 6CFRP10a with a 0.5 mm face sheet thickness, while face sheet material damage was determined in the specimens with thicknesses of 1 and 1.5 mm.

The first damage type seen in core the beginning of the test is cracks in the cell walls. With the continuation of the test, crushing of the cell walls and adhesive damage of the cell walls were observed. With the catastrophic failure seen in the samples, the damage has been concentrated especially in the support areas.

Figure 6 shows applied force vs. deflection graphs for specimens with aluminum and CFRP face sheet materials. For both face sheet materials, increasing face sheet thickness increased flexural strength. Moreover, for the same load values, deflection decreased due to increased face sheet thickness. For example, in the specimens with an aluminum face sheet, the amounts of deflection under a 2000 N load were measured to be 1.133 mm, 0.917 mm and 0.524 mm for 6AL10a, 6AL10b and 6AL10c specimens, respectively.

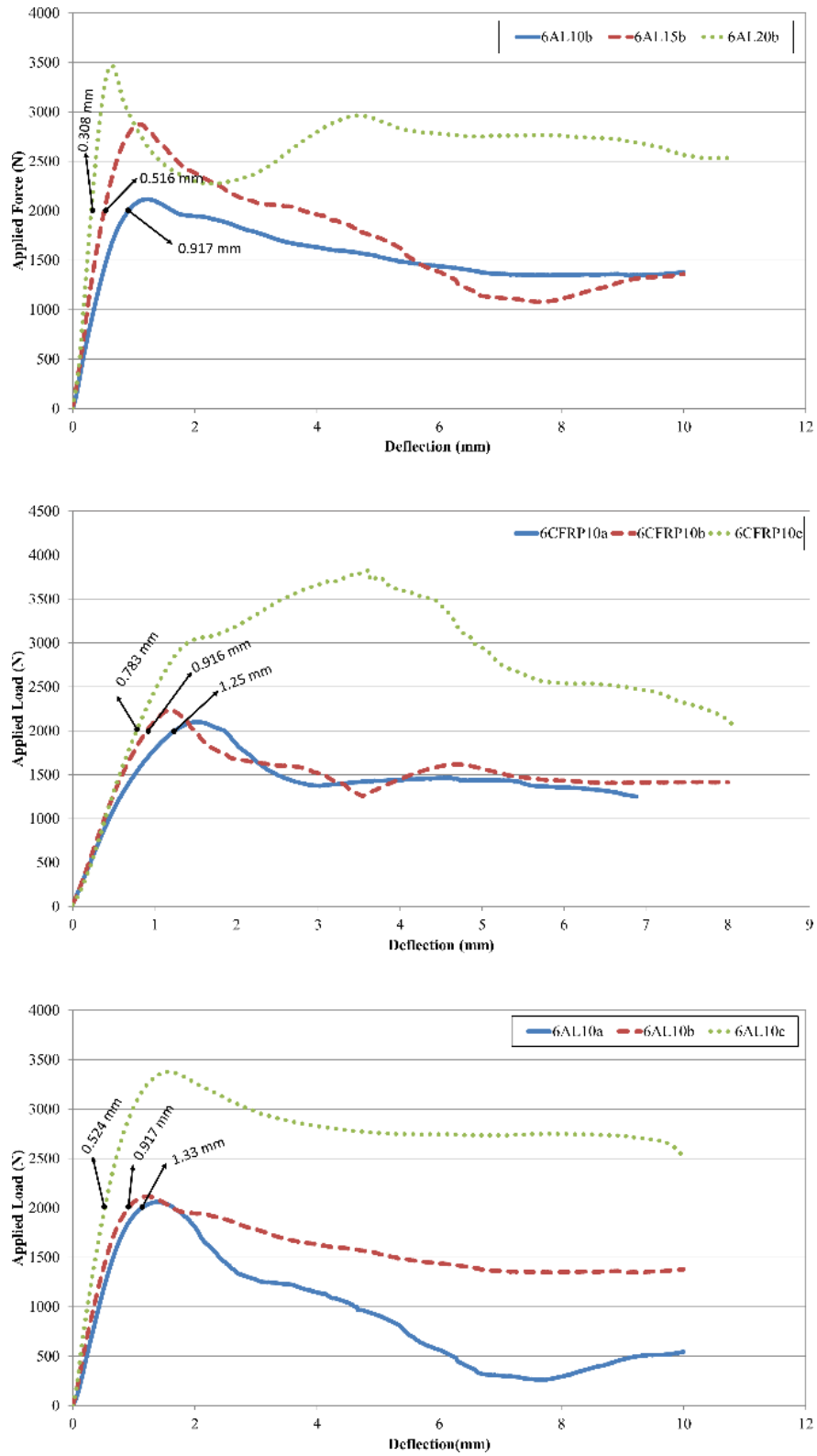


Figure 6. Effect of face sheet thickness, type and core height on flexural strength

Increased face sheet thickness reduced the amount of damage formed on the face sheet after impact tests. Similarly, increasing face sheet thickness decreased flexural strength more after impact. The reason for this was that during impact loading on increasing face sheet thicknesses, more of the applied load was transferred to the cores.

4.2. Fatigue Tests

Impact failure may happen any time during the lifetime of the structures. Impact failure can be observed aviation structures such as airplanes due to bird strikes or collision of ground vehicles. Main aim of this paper is to investigate the effect of impact damage on the fatigue life of honeycomb sandwich structures. The fact that impact damage was not examined for the later stages of fatigue damage constitutes the missing aspect of this study. Sandwich structures suffers not only bending loads but also compression or membrane stretch loads.

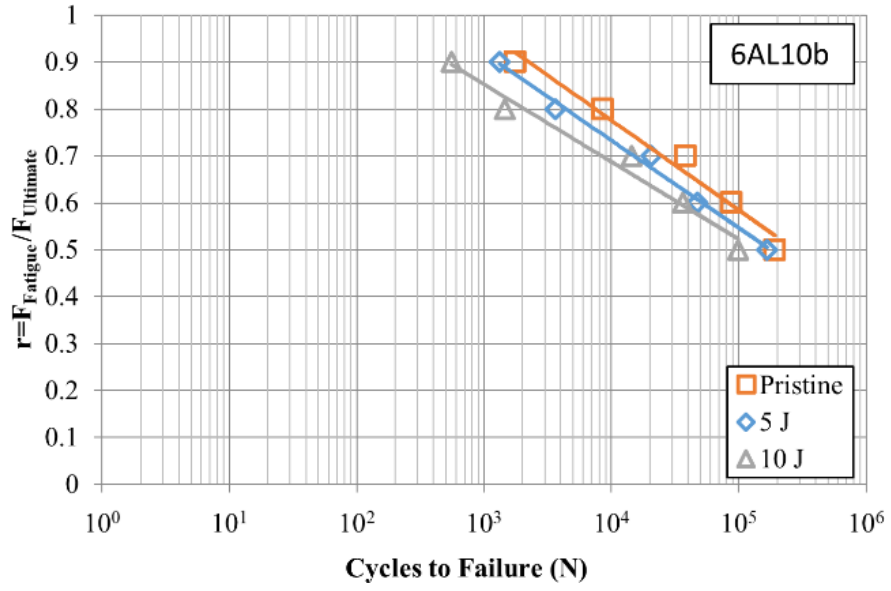
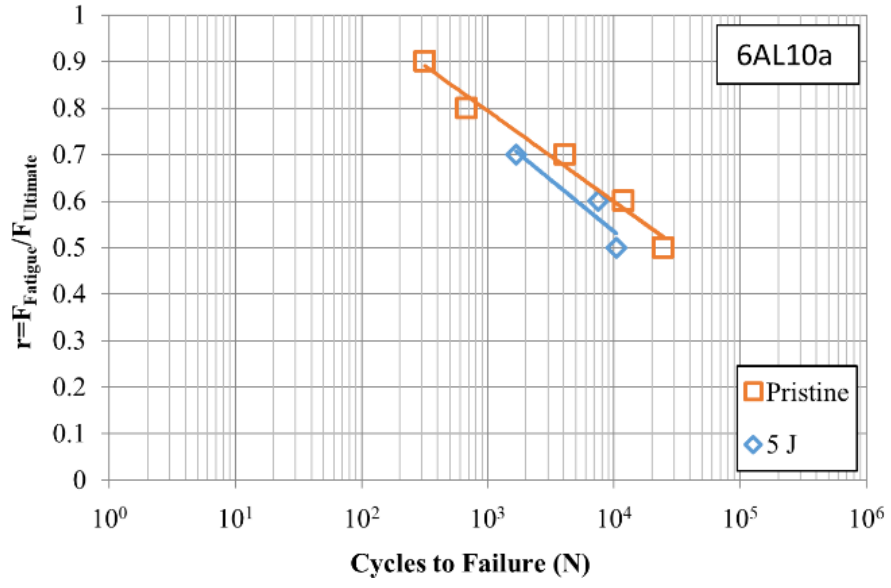
Sandwich composites, whose strength values were determined by static tests, were subjected to testing both without impact and with impacts of variable energies; after that, fatigue tests were carried out. For fatigue tests, three-point bending loads were applied to specimens as for the static tests. Damaged specimens were subjected to fatigue tests using the load values determined by the static values of undamaged specimens. The reason for this was to determine changes in fatigue behaviors of damaged specimens with respect to undamaged specimens.

All fatigue tests were repeated three times and mean values were used, while fatigue graphs were drawn to avoid confusion. Because of decreases in the strengths of specimens with preliminary impact damage, fatigue tests were not performed for some values.

Figure 7 (a) shows the fatigue graphs of specimen 6AL10a with a 0.5 mm-thick aluminum face sheet obtained under three-point bending loads. It was seen that impact testing decreased the fatigue strength of specimens for all loading ratios. Reductions in fatigue strength increased as the applied loading ratio ($r = F_{\text{fatigue}}/F_{\text{ultimate}}$) increased. The greatest fatigue life decrease (59%) was determined at $r = 0.7$.

Figure 7 (b) shows the loading ratio vs. cycles to failure graphs for 6AL10b specimens obtained from fatigue tests. Decreasing the loading ratio decreased the impact effect. For a loading ratio of 0.9, the average life of undamaged specimens was 1767 cycles, while the average life of the specimen damaged by 10 Joules of impact energy decreased by 69%, or 556 cycles. When the loading ratio was 0.5, the reduction was 49%.

Figure 7 (c) shows graphs with cycles to failure corresponding to different loading ratios for the 6AL10c specimen. For all loading ratios, the fatigue lives of damaged specimens were lower. Increasing the fatigue load increased the difference between undamaged and damaged specimens. Decreasing the applied load decreased the strength reduction in damaged specimens.



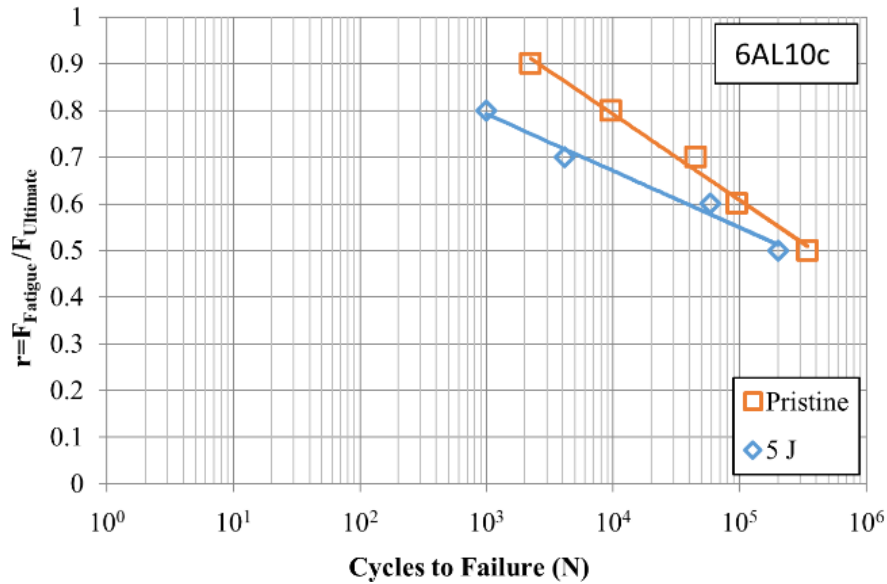
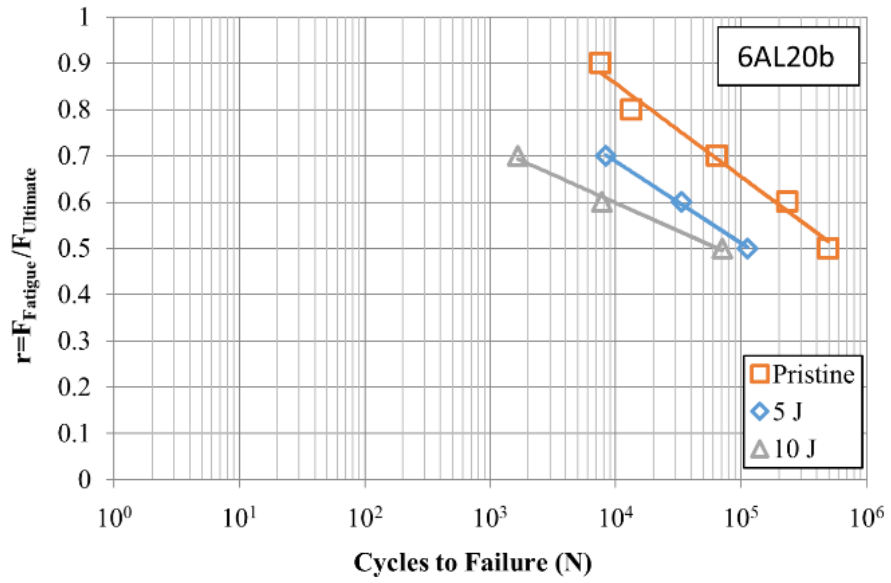
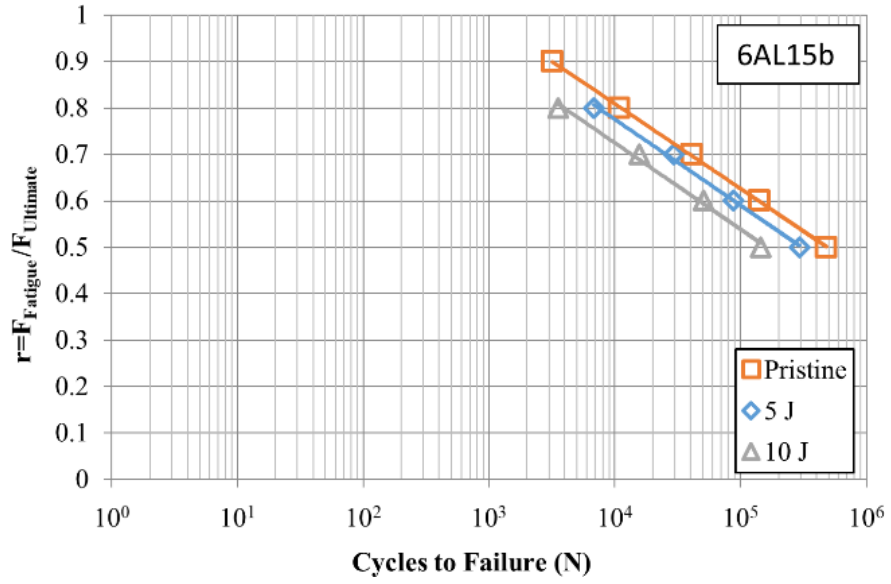


Figure 7. Loading ratio vs. cycles to failure graphs for (a) 6AL10a, (b) 6AL10b and (c) 6AL10c specimens

Figure 8 (a) shows cycles to failure values corresponding to different loading ratios for the 6AL15b specimen. For all loading ratios, the cycles to failure value of specimens damaged with 5 Joules of impact energy was approximately 62% of undamaged specimens. Similarly, the cycles to failure value for specimens damaged with 10 Joules of impact energy was approximately 50% of undamaged specimens. This shows that the relationship between impact energy and fatigue life is not linear.

Figure 8 (b) shows cycles to failure values corresponding to different loading ratios for the 6AL20b specimen. The specimen affected most by preliminary damage was 6AL20b. For $r = 0.7$, the preliminary damage produced by 5 Joules and 10 Joules of impact energy decreased the specimen's life by 85% and 97.5% compared to that of the undamaged specimen. Decreasing the loading ratio increased the life of damaged and undamaged specimens.

Figure 8 (c) shows cycles to failure values corresponding to loading ratios for the 9AL10b specimen. The static damage load of the specimen for 5 Joules of impact energy was 1739 N, while it decreased to 1539 N for 10 Joules of impact energy. When fatigue tests were performed at 90% and 80% of the static damage value for undamaged specimens, the applied static loads were found to be 1750 N and 1550 N, respectively. The static damage loads for specimens damaged by 5 Joules of impact energy were below 90% of the static damage load of the undamaged specimen, while those damaged by 10 Joules of impact energy were below 90% and 80% of the static damage load of the undamaged specimen. Thus, the fatigue tests were not carried out at these loading ratios.



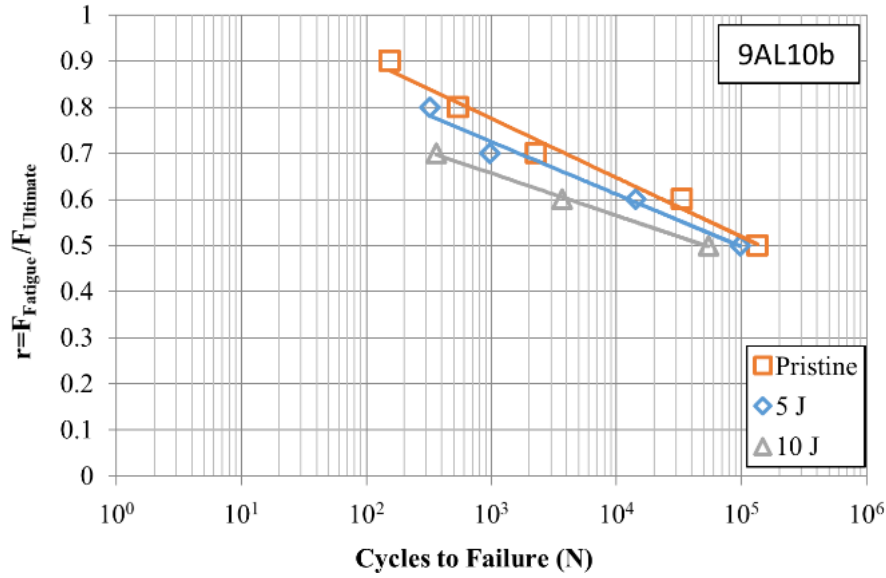
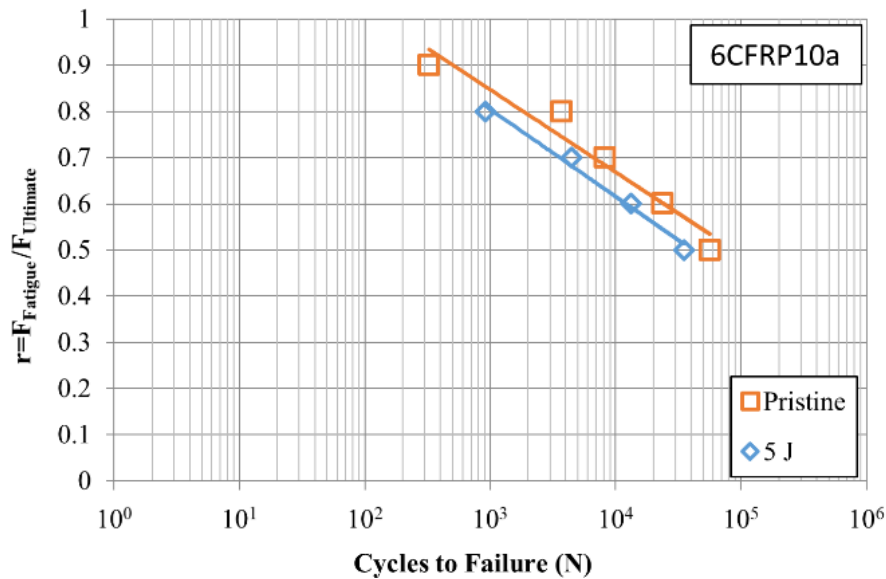


Figure 8. Loading ratio vs. cycles to failure graphs for the (a) 6AL15b, (b) 6AL20b and (c) 9AL10b specimens

Figure 9 shows the fatigue test results for the 6CFRP10a, 6CFRP10b and 6CFRP10c specimens. It was seen that the specimen affected most by the preliminary impact damage was 6CFRP10c with a face sheet material thickness of 1.5 mm. The reason for this could be that increasing face sheet thickness increased the preliminary damage resistance of the face sheet, which caused more cores to be crushed. Cycles to failure values determined in 6CFRP10b specimen damaged by 5 Joules of impact energy diverged from the cycles to failure value of the undamaged specimen due to the decreasing loading ratio. Loading ratio vs. cycles to failure graph of specimens damaged by 10 Joules of energy corresponded to that of the undamaged specimen.



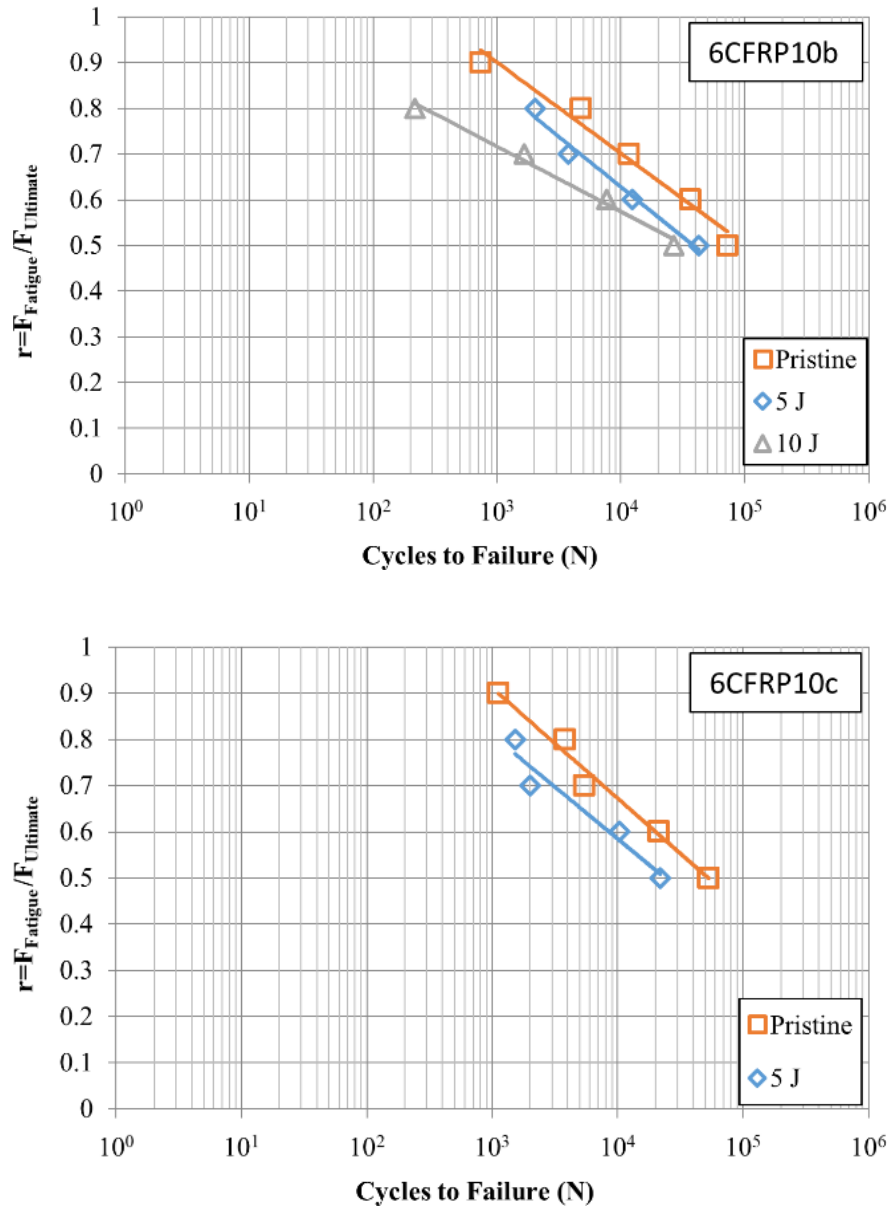


Figure 9. Loading ratio vs. cycles to failure graphs for the (a) 6CFRP10a, (b) 6CFRP10b and (c) 6CFRP10c specimens

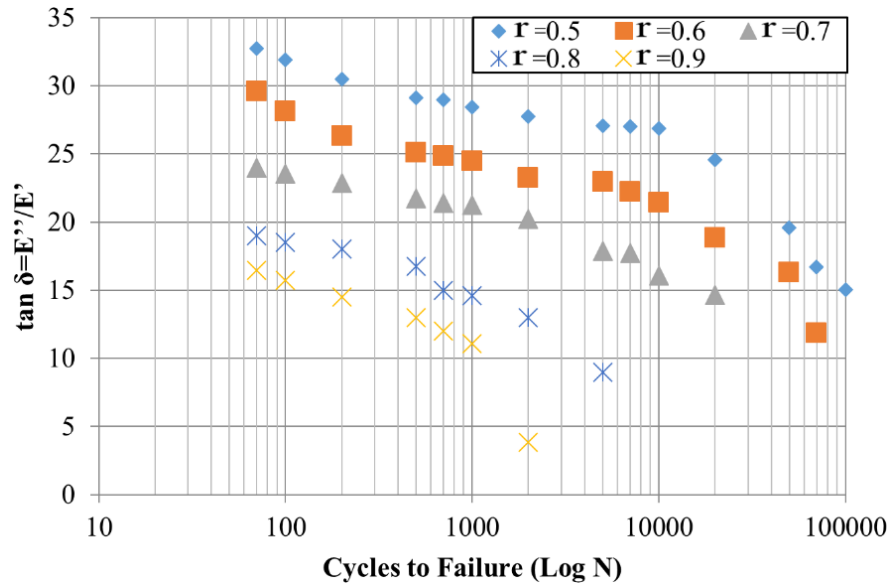
Fatigue crack didn't observed during fatigue tests due to loading type. Core crushing failure is the main failure type for all fatigue specimens. No failures observed for adhesive between core and face material. Adhesion tests can be investigated in future studies.

4.3. Damping Ratio and Stiffness Reduction

Damping indicates the amount of energy required to rearrange molecules of the material due to internal friction. The energy consumed by the material due to internal friction and movements is called the loss modulus (E''), while the response energy consumed by the material against impact is the damping modulus (E''). The damping ratio is calculated by the formula $\tan(\delta) = E''/E'$, and it is independent of geometric effects.

To determine the amount of energy absorbed by specimens after the fatigue tests, $\tan(\delta)$ vs. cycles to failure ($\log N$) graphs are shown below.

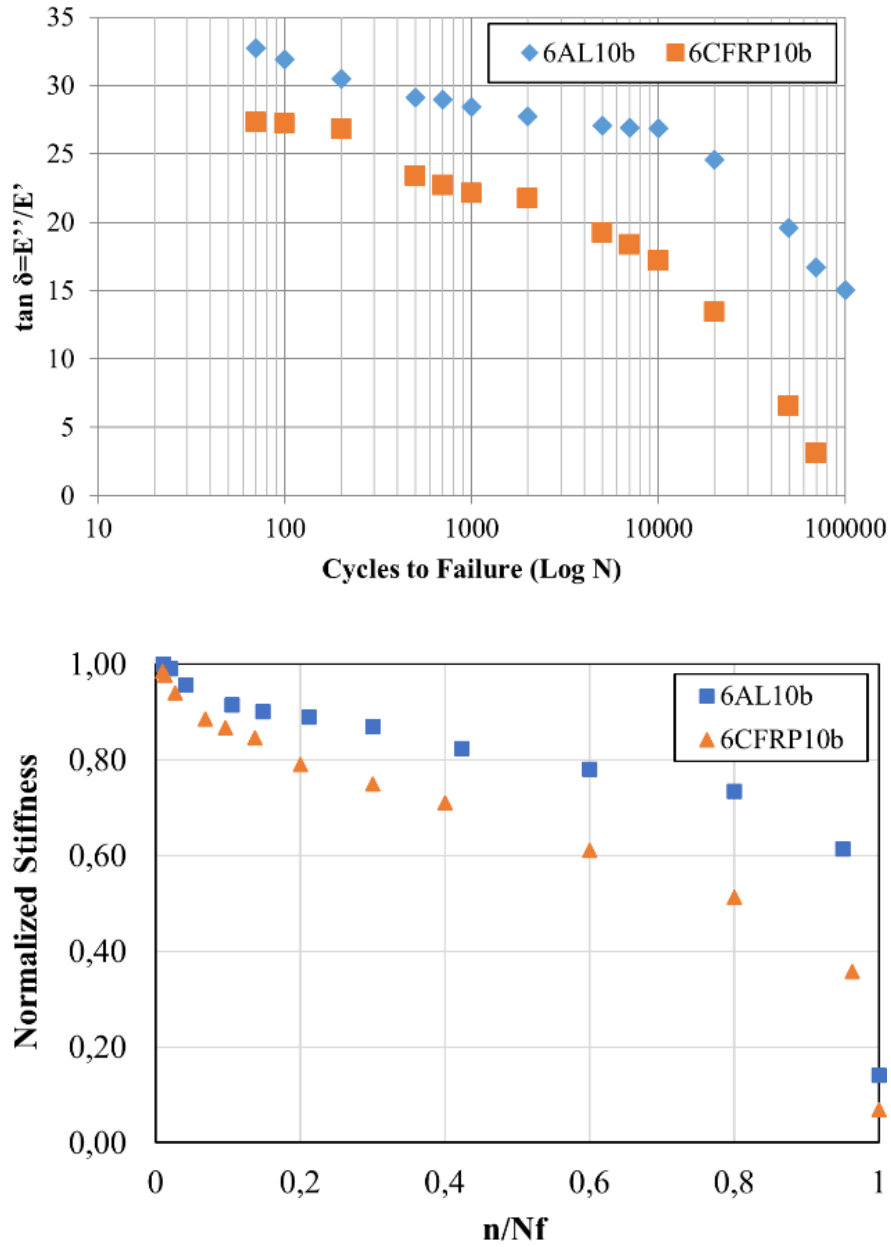
Figure 10 shows the effect of different loading ratios on the damping ratio for the undamaged 6AL10b specimen under three-point bending loads. The damping ratio decreased with increasing loading ratio, while for all loading ratios, minimum damping ratios were determined at cycles to failure values where fatigue damage occurred.



Φιγυρε 10. Ταν (δ) ς. Λογ (N) γραπη φορ τηε 6AL10β σπεεεμεν

Figure 11 (a) shows damping ratios of the 6AL10b and 6CFRP10b specimens at a loading ratio of $r = 0.6$. At the same loading ratio, the damping ratios of the aluminum specimen were found to be higher than those of the CFRP specimen.

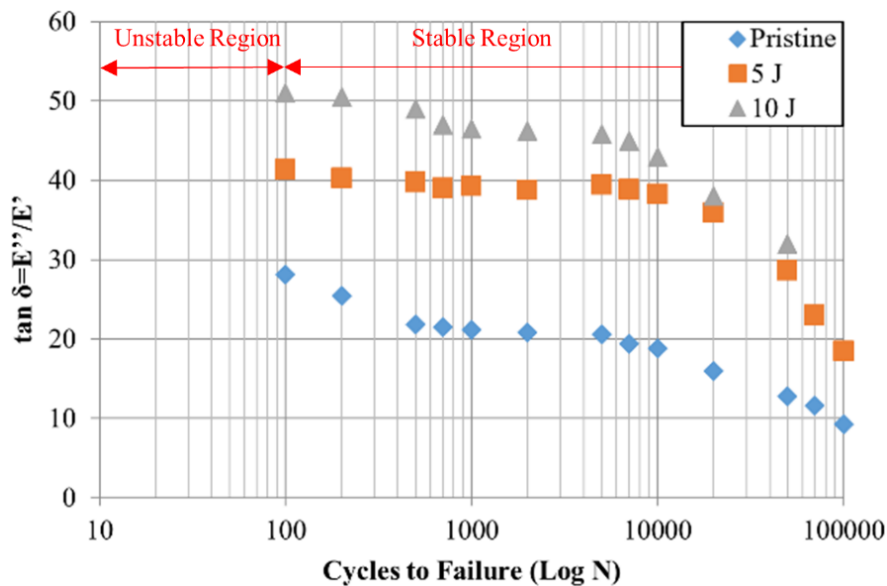
Figure 11 (b) shows the normalized cycle – Stiffness reduction graph for 6AL10b and 6CFRP10b specimens. Stiffness calculated as maximum applied load divided by maximum deflection for every cycle³¹. Stiffness change with fatigue cycle shows the same trend with damping ratio graphs. While normalized fatigue cycle approaching the 1, stiffness decreases and dramatical stiffness reduction observed at the end of lifetime.



Φιγυρε 11. (α)Ταν (δ) ς. Λογ (N) γραπη φορ τη 6ΑΛ10β ανδ 6ΦΡΠ10β σπεσιμενς, (β) Στιφυνες ρεδυστιον ς νορμαλιζεδ ςψςλε γραπη φορ 6ΑΛ10β ανδ 6ΦΡΠ10β σπεσιμενς

Figure 12 shows the effect of impact energy on the damping ratio for the 9AL10b specimen. Increasing impact energy increased the damping ratio while increasing cycles to failure decreased the damping ratio. After 100 cycles, when the stable region starts, the reduction in the damping ratio of damaged specimens (5 Joules and 10 Joules) was less compared to the undamaged specimen.

Damping ratio of undamaged specimens was lower than that of damaged specimens (Figure 10). The reason for this may be that undamaged structure transmits vibration more ³².



Φιγυρε 12. Ταν (δ) ς. Λογ (N) γραπη φορ τη 9AL10β σπεριμεν

Conclusion

The results obtained after three-point bending, low velocity impact, three-point bending after impact, fatigue and fatigue after impact tests are evaluated below:

- For three-point bending loads, increasing the core height increased the damage load of the specimen. With increased core height, damage was concentrated on the zone affected by the load. For the three core height values, debonding damage was seen between the core and the face sheet; buckling of the cell walls is the main reason for the damage.
- Increasing face sheet thickness increased flexural strength of specimens for both face sheet materials. This increase was more apparent in specimens of CFRP.
- While performing fatigue tests, the applied load was determined by using the static damage load of the specimen. This restricted the effect of parameters used in the study on fatigue behavior. Application of the same amount of load to all specimens will clarify the effects of these parameters on fatigue behavior.
- Increasing the core height was found to be the parameter that increased fatigue strength of specimens the most, similar to static loading.
- In fatigue tests performed by three-point bending tests, when the loading ratio decreased, the fatigue lives of undamaged and damaged specimens converged.
- The damping ratio – related to the energy absorbed by specimens during fatigue tests and to rigidity – increased with increasing impact energy. For undamaged and damaged specimens, the damping ratio approached a steady-state and continued its horizontal trend; it decreased when approaching the damage cycle and became a minimum after permanent damage of the specimen.
- For all cycle numbers, the highest damping ratios were observed in specimens with the aluminum face sheet.
- While normalized fatigue cycle approaching the 1, stiffness decreases and dramatical stiffness reduction observed at the end of lifetime for all samples.

Acknowledgments

This work was supported by Scientific Research Projects Coordination Unit of Firat University. Project

number MF.16.18. Tolga TOPKAYA is grateful to The Scientific and Technological Research Council of Turkey (TUBITAK) for Ph.D. scholarship (Grant Number: 1649B031501671).

This paper is a part of 479133 numbered and “Investigation of the fatigue behavior of honeycomb sandwich composites after low-velocity impact damage” titled Ph. D. thesis of Dr. Tolga TOPKAYA, awarded from Firat University Graduate School of Sciences.

References

1. Rajaneesh A, Zhao Y, Chai GB, et al. Flexural fatigue life prediction of CFRP-Nomex honeycomb sandwich beams. *Compos Struct* 2018; 192: 225–231.
2. Wu X, Yu H, Guo L, et al. Experimental and numerical investigation of static and fatigue behaviors of composites honeycomb sandwich structure. *Compos Struct* 2019; 213: 165–172.
3. Hajmohammad MH, Kolahchi R, Zarei MS, et al. Dynamic response of auxetic honeycomb plates integrated with agglomerated CNT-reinforced face sheets subjected to blast load based on visco-sinusoidal theory. *Int J Mech Sci* 2019; 153–154: 391–401.
4. Yang FP, Lin QY, Jiang JJ. Experimental study on fatigue failure and damage of sandwich structure with PMI foam core. *Fatigue Fract Eng Mater Struct* 2015; 38: 456–465.
5. Strek T, Jopek H, Nienartowicz M. Dynamic response of sandwich panels with auxetic cores. *Phys Status Solidi Basic Res* 2015; 252: 1540–1550.
6. Pehlivan L, Baykasoğlu C. An experimental study on the compressive response of CFRP honeycombs with various cell configurations. *Compos Part B Eng* 2019; 162: 653–661.
7. Akpınar S, Aydın MD, Temiz Ş, et al. 3-D non-linear stress analysis on the adhesively bonded T-joints with embedded supports. *Compos Part B Eng* 2013; 53: 314–323.
8. Belouettar S, Abbadi A, Azari Z, et al. Experimental investigation of static and fatigue behaviour of composites honeycomb materials using four point bending tests. *Compos Struct* 2009; 87: 265–273.
9. Wu Y, Liu Q, Fu J, et al. Dynamic crash responses of bio-inspired aluminum honeycomb sandwich structures with CFRP panels. *Compos Part B Eng* 2017; 121: 122–133.
10. Quispitupa A, Berggreen C, Carlsson LA. Face/core interface fracture characterization of mixed mode bending sandwich specimens. *Fatigue Fract Eng Mater Struct* 2011; 34: 839–853.
11. Nouri H, Lubineau G, Traudes D. An experimental investigation of the effect of shear-induced diffuse damage on transverse cracking in carbon-fiber reinforced laminates. *Compos Struct* 2013; 106: 529–536.
12. Zhang W, Zhou Z, Zheng P, et al. The fatigue damage mesomodel for fiber-reinforced polymer composite lamina. *J Reinf Plast Compos* 2014; 33: 1783–1793.
13. Kolahchi R, Cheraghbak A. Agglomeration effects on the dynamic buckling of viscoelastic microplates reinforced with SWCNTs using Bolotin method. *Nonlinear Dyn* 2017; 90: 479–492.
14. Motezaker M, Jamali M, Kolahchi R. Application of differential cubature method for nonlocal vibration, buckling and bending response of annular nanoplates integrated by piezoelectric layers based on surface-higher order nonlocal-piezoelasticity theory. *J Comput Appl Math* 2020; 369: 112625.
15. Wang Z, Li Z, Zhou W, et al. On the influence of structural defects for honeycomb structure. *Compos Part B Eng* 2018; 142: 183–192.
16. Jen YM, Ko CW, Lin H Bin. Effect of the amount of adhesive on the bending fatigue strength of adhesively bonded aluminum honeycomb sandwich beams. *Int J Fatigue* 2009; 31: 455–462.
17. Subhani T. Mechanical Performance of Honeycomb Sandwich Structures Using Three-Point Bend Test. 2019; 9: 3955–3958.

18. Jen YM, Chang LY. Effect of thickness of face sheet on the bending fatigue strength of aluminum honeycomb sandwich beams. *Eng Fail Anal* 2009; 16: 1282–1293.
19. Abbadi A, Tixier C, Gilgert J, et al. Experimental study on the fatigue behaviour of honeycomb sandwich panels with artificial defects. *Compos Struct* 2015; 120: 394–405.
20. Schubel PM, Luo JJ, Daniel IM. Impact and post impact behavior of composite sandwich panels. *Compos Part A Appl Sci Manuf* 2007; 38: 1051–1057.
21. Belingardi G, Martella P, Peroni L. Fatigue analysis of honeycomb-composite sandwich beams. *Compos Part A Appl Sci Manuf* 2007; 38: 1183–1191.
22. Shi SS, Sun Z, Hu XZ, et al. Carbon-fiber and aluminum-honeycomb sandwich composites with and without Kevlar-fiber interfacial toughening. *Compos Part A Appl Sci Manuf* 2014; 67: 102–110.
23. Akatay A, Bora MÖ, Çoban O, et al. The influence of low velocity repeated impacts on residual compressive properties of honeycomb sandwich structures. *Compos Struct* 2015; 125: 425–433.
24. Galehdari SA, Kadkhodayan M, Hadidi-Moud S. Low velocity impact and quasi-static in-plane loading on a graded honeycomb structure; experimental, analytical and numerical study. *Aerosp Sci Technol* 2015; 47: 425–433.
25. Baba BO. Curved sandwich composites with layer-wise graded cores under impact loads. *Compos Struct* 2017; 159: 1–11.
26. He W, Yao L, Meng X, et al. Effect of structural parameters on low-velocity impact behavior of aluminum honeycomb sandwich structures with CFRP face sheets. *Thin-Walled Struct* 2019; 137: 411–432.
27. Longbiao L. A hysteresis energy dissipation based model for multiple loading damage in continuous fiber-reinforced ceramic-matrix composites. *Compos Part B Eng* 2019; 162: 259–273.
28. Menard KP. *Dynamic Mechanical Analysis: A Practical Introduction*. CRC Press, 2008.
29. De Silva CW. *Dynamic testing and seismic qualification practice*. Carnegie-Mellon Univ, 1983.
30. Topkaya T, Solmaz MY. Investigation of low velocity impact behaviors of honeycomb sandwich composites. *J Mech Sci Technol* 2018; 32: 3161–3167.
31. Suzuki T, Mahfuz H, Takanashi M. A new stiffness degradation model for fatigue life prediction of GFRPs under random loading. *Int J Fatigue* 2019; 119: 220–228.
32. Idriss M, El Mahi A, Assarar M, et al. Damping analysis in cyclic fatigue loading of sandwich beams with debonding. *Compos Part B Eng* 2013; 44: 597–603.